Seasonal variability and predictability of monsoon precipitation in Southern Africa

Matthew F. Horan[1,2], Fred Kucharski [3], Moetasim Ashfaq[1]

[1] *Computational Sciences and Engineering Division, Oak Ridge National Laboratory, Oak Ridge, Tennessee, United States*

[2] *Bredesen Center, University of Tennessee, Knoxville, Tennessee, United States*

[3] *Earth System Physics, Abdus Salam International Centre for Theoretical Physics, Trieste, Italy*

[4] *National Oceanic and Atmospheric Administration/Geophysical Fluid Dynamics Laboratory, Princeton, NJ, USA*

Key Points:

- An empirical model using three tropical forcings accurately describes 50–80% of peak monsoon precipitation variability in Southern Africa.
- Significant prediction skill exists with up to five months lead time, which is weakest when the identified forcings are highly correlated
- Seasonal forecast systems underperform the empirical model as they skillfully represent the forcings but lack accuracy in teleconnections.

Abstract

Rainfed agriculture is the mainstay of economies across Southern Africa (SA), where most precipitation is received during the austral summer monsoon. Despite that, seasonal precipitation predictability in SA is less explored. Here we use three natural climate forcings, El Niño–Southern Oscillation (ENSO), Indian Ocean Dipole (IOD), and the Indian Ocean Precipitation Dipole (IOPD) – the dominant precipitation variability mode – to construct an empirical model that exhibits significant skill over SA during monsoon in explaining precipitation variability and in forecasting it with a five-month lead. While most explained precipitation variance (50–75%) comes from contemporaneous IOD and IOPD, preconditioning all three forcings is key in predicting monsoon precipitation with a zero to five-month lead. Seasonal forecasting systems accurately represent the interplay of the three forcings but show varying skills in representing their teleconnection over SA. This makes them less effective at predicting monsoon precipitation than the empirical model.

Plain Language Summary

Accurately predicting precipitation is crucial for agricultural planning in Southern Africa (SA), as the region is prone to droughts and floods. Here we develop an empirical model employing sea surface temperature and precipitation indexes from the Pacific and Indian Oceans to forecast average precipitation in SA from December through February. It can account for approximately half of the variation in Southern African precipitation with a five-month lead time and about three-fourths of the variation using December preconditions. The empirical model outperforms seasonal forecast systems when considering the same lead times. Although seasonal forecast systems can skillfully predict modes of variability related to sea surface temperatures and precipitation in the two oceanic basins, they are less consistent in predicting the relationship between their indexes and precipitation over Southern Africa. Specifically, they show a stronger correlation between Pacific Ocean temperatures and Southern African precipitation and too weak correlation with the Indian Ocean.

1 Introduction

Southern Africa (SA) is a drought- and flood-prone region of the world where over 95% of agriculture relies on seasonal precipitation primarily occurring during the austral summer monsoon (Ashfaq et al., 2020; Mpungose et al., 2022; Reason & Rouault, 2002; Wetterhall et al., 2014; Winsemius et al., 2014). Most of the precipitation during the peak of the monsoon season (December to February) is enhanced by tropical lows and, in some cases, tropical cyclones that form within the tropics and move westward over Africa (Barimalala et al., 2020; Howard et al., 2019; Ibebuchi, 2023a).

Earlier studies suggested that El Niño–Southern Oscillation (ENSO) and Indian Ocean Dipole (IOD) are the two primary mechanisms contributing to SA monsoon seasonal variability (Crétat et al., 2019; Howard et al., 2019; Ibebuchi, 2023b; Manatsa et al., 2012; Reason & Jagadheesha, 2005), while Madden Julian Oscillation (MJO) is responsible for intraseasonal variability (De Andrade et al., 2021; Silvério & Grimm, 2022). Beyond providing contemporaneous forcing, the IOD has also been shown to predict austral summer precipitation with several months lead (Ibebuchi, 2023b). However, IOD and ENSO are usually not independent of each other. Therefore, it is only possible to independently attribute precipitation variability to one with accounting for the other's influence. Recent studies also suggest that the leading mode of precipitation variability in the Indian Ocean (IO) mediates tropical forcings effects in distant regions (Abid et al., 2020, 2023; Horan et al., 2023; Mehmood et al., 2022). However, it is currently unknown whether it plays a role in mediating ENSO and IOD influences over SA during monsoon or has a distinct role that can be leveraged to predict monsoon precipitation.

Accurate seasonal predictability of monsoon precipitation across SA can be a key to sustainable agricultural practices. Evidence of seasonal precipitation predictability over parts of SA relates to Pacific and Indian oceans Sea Surface temperature (SST) variability (De Andrade et al., 2021; Ibebuchi, 2023b; Landman et al., 2012; Monerie et al., 2019; Reason et al., 2006). However, neither the sources of predictability nor empirical and dynamical models have been fully exploited for predicting monsoon precipitation in SA (Landman et al., 2012; Landman & Beraki, 2012; Munday & Washington, 2017). To further our understanding of the SA monsoon, we develop an empirical model using ENSO, IOD, and the dominant precipitation mode in the IO as leading precursors and contemporaneous forcings. This model examines the roles of these factors in precipitation variability and predictability across SA. In addition, we analyze the skillfulness of two seasonal forecasting systems, the Geophysical Fluid Dynamics Laboratory (GFDL) Seamless System for Prediction and Earth System Research (SPEAR; Delworth et al., 2020) and the European Center for Medium-Range Weather Forecasts (ECMWF) fifth-generation seasonal forecasting system (SEAS5; Johnson et al., 2019), in predicting monsoon over SA with initializations at zero-, two-, and five-months lead. We aim to answer two key questions using this analytical framework: 1) What are the roles of ENSO, IOD, and the dominant IO precipitation mode in monsoon precipitation variability and predictability over SA? How effective are SPEAR and SEAS5 in predicting summer monsoon over SA, and can their skillfulness or lack thereof be explained by their capability or shortcoming to represent the influences of these three natural forcings?

2 Data and Methods

This study uses precipitation and atmospheric variables from ECMWF’s Fifth Generation Reanalysis (ERA5; Hersbach et al., 2020) for data consistency required in teleconnection analyses (Mukherjee et al., 2020). We analyze monthly precipitation, SST, and three-dimensional atmospheric winds, divergence, and vertical pressure velocity. ERA5 precipitation compares reasonably with the Climate Research Unit (CRU) Timeseries 4.07. (Harris et al., 2020). However, a substantial disparity exists between CRU and Climate Prediction Center (CPC; Xie et al., 2007) over SA (Figure S1), with CPC being substantially drier.

Moreover, two seasonal forecasting systems are analyzed for their skillfulness in predicting the SA monsoon: GFDL’s SPEAR with 15 members and ECMWF's SEAS5 with 25 members. We use zero-, two-, and five-month lead simulations, initialized in December, October, and July for SPEAR, while SEAS5 only has data for zero- and two-month lead simulations, initialized in December and October. The analysis period covers 1991 through 2022, which overlaps in all three datasets (ERA5, SEAS5, and SPEAR). All data is linearly detrended before use except for climatological analyses.

The analyses cover land areas south of 5°S for the austral summer months (December to February; DJF). While the rainy season substantially varies latitudinally across SA, DJF is the region's core monsoon season (Ashfaq et al., 2020). We investigate monsoon precipitation variability and predictability using three natural modes of variability: ENSO, IOD, and the dominant mode of precipitation variability in the IO, hereafter termed the IO Precipitation Dipole (IOPD; Horan et al., 2023). We define the ENSO index as the Principal Component (PC) of the first Empirical Orthogonal Function (EOF) of monthly SSTs in the Pacific covering 160°W–80°E and 10°S–10°N (Figure S2). The PC-based ENSO index strongly correlates with SST-based Niño indexes. It is preferred over choosing one of the four Niño indexes to minimize issues related to ENSO diversity. The IOD (Saji et al., 1999) is defined using the standardized difference in SSTs between the Western (50°E–70°E, 10°S–10°N) and Eastern (90°E–110°E, 10°S–0°) IO. Some studies have used the Subtropical IOD (SIOD) index to investigate SA's precipitation variability (Behera & Yamagata, 2001; Hoell et al., 2017; Ibebuchi, 2023a; Reason, 2001). Our analyses didn't find it more relevant than IOD (not shown). IOPD is the PC of the first EOF of monthly precipitation in the IO, covering 40°E–140°E and 10°S–10°N (Figure S1; Horan et al., 2023).

We use multiple linear regression (MLR), simple Pearson correlation, and partial correlation analyses to investigate the individual and combined influences of three modes of variability on SA monsoon precipitation. A two-tailed T-test determines the significance of regression coefficients, while an F-test determines the added value of each independent variable in the MLR model. All results are tested for significance at 95% confidence. The MLR model is further tested for overfitting by comparing the coefficient of determination (R^2) and predicted R^2. For calculating predicted R^2, we remove each data point from the time series at each grid point, calculate the regression equation, and subsequently use that equation to predict the removed data point. The process is repeated for each data point until we have a time series that is completely predicted based on the regression model.

3 Results and Discussion

The rainy season in SA varies significantly with latitude, from three months south of 20°S to over six months at 10°S (Figure 1a). The seasonal march of monsoon rains over SA starts in November (Figures 1a, S1, S3), the onset month (Ashfaq et al., 2020). DJF is the core monsoon season as zonal average precipitation exceeds 2 mm/day throughout the latitudinal belt between 5°S and 30°S. Monsoon withdraws from most of the region in March (Figure S3; Ashfaq et al., 2020). The seasonal maximum of average precipitation and its variability occurs at the boundary of the dryline or Congo air boundary (Figure 1b, 1c; Howard & Washington, 2019). A comparable seasonal precipitation distribution with a low interannual variability is also observed between northern Mozambique and Angola. South of that, precipitation exhibits a latitudinally expanding east-west

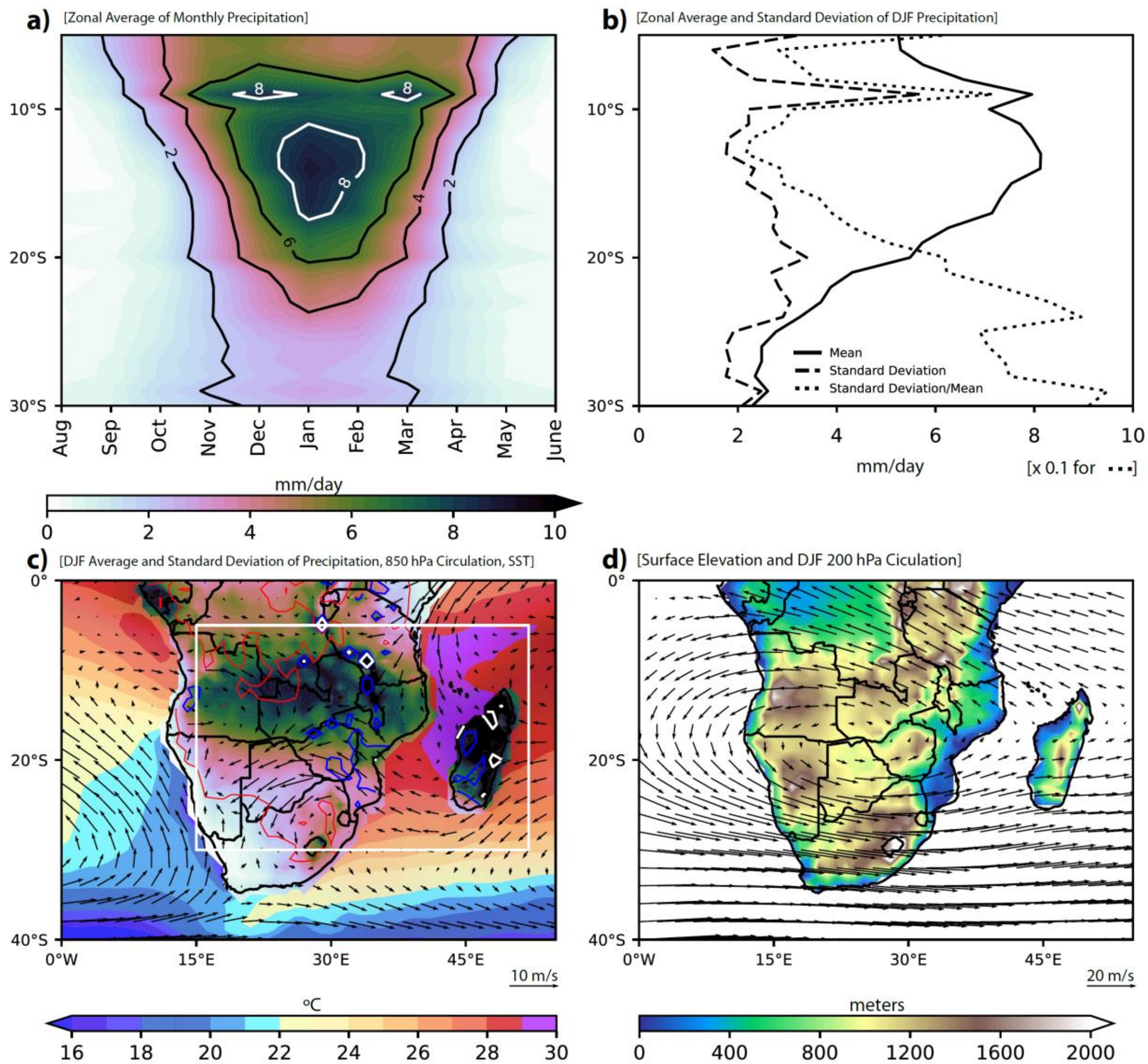

Figure 1. Zonally averaged (5°E–52°E, land points) monthly precipitation (a), DJF mean, and standard deviation of precipitation, along with the ratio of standard deviation to the mean (b). c) Color contours: DJF surface temperature (ocean) and precipitation (land), line contours: DJF precipitation standard deviation (red, blue, white: 1, 2, 3 mm/day), vectors: winds at 850 hPa. The white box indicates the core study area. d) 200 hPa winds and topography over Southern Africa. Analyses cover 1991–2022 in ERA5.

gradient with higher magnitudes east of the Kalahari Desert and little precipitation in its west. The proportion of precipitation variability relative to the mean increases over regions south of 15°S (Figure 1b). The north-south precipitation gradient also extends from mainland Africa to Madagascar. SA receives the most moisture from continental recycling, while the warm IO (Figure 1c) contributes the major oceanic moisture source to continental precipitation (Geppert et al., 2022). Several key dynamical features regulate the spatially complex distribution of monsoon precipitation over SA. In the lower atmosphere (850 hPa), these features include the Angolan Low

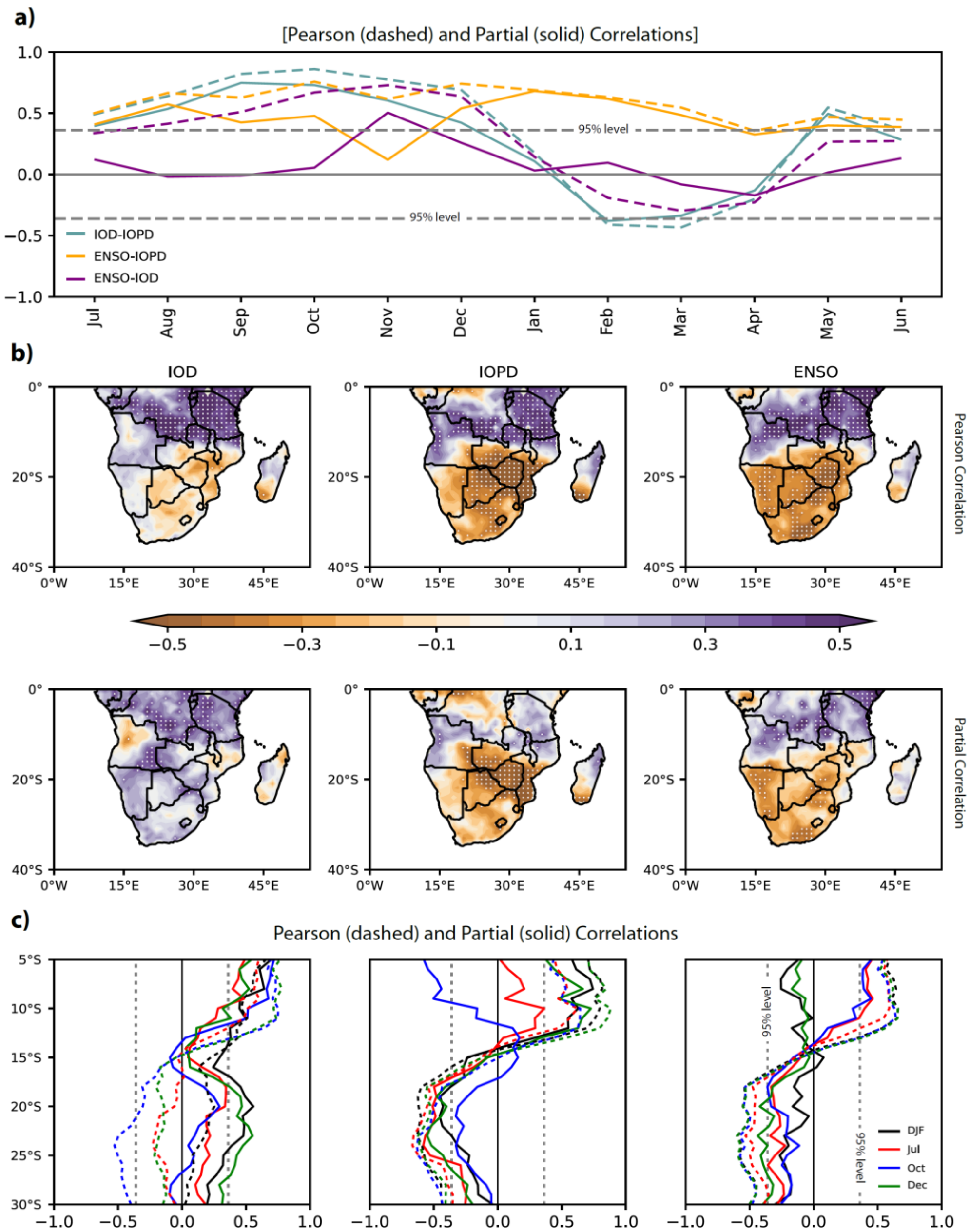

Figure 2. a) The monthly Pearson (dashed) and partial (solid) correlation between ENSO, IOD, and IOPD. b) DJF Pearson (second row) and partial (third row) correlations between precipitation over Southern Africa and IOD (left), IOPD (center), and ENSO (right). c) Zonal average of Pearson (dashed) and partial (solid) correlations of DJF precipitation (5°E–52°E, land points) with DJF, December, October, and July indexes of IOD, IOPD, and ENSO. Stippling in (b) and vertical dashed lines in (c) represent statistical significance (p<.05).

(AL) in the northwest, the Mozambique Channel Trough (MCT) between central Mozambique and Madagascar, and the diagonally oriented South Indian Convergence Zone (SICZ) off the southeast coast of SA (Figure 1c). The upper atmosphere circulations (200 hPa; Figure 1d) are characterized by a high extending between the South Atlantic and Indian oceans with an approximate center at the border of Zambia, Botswana, and Zimbabwe, commonly called the Botswana High (BH). The role of these dynamical features in maintaining the summer monsoon over SA has been described extensively in several earlier studies (Barimalala et al., 2020; Cook, 2000; Crétat et al., 2019; Driver & Reason, 2017).

Several studies have investigated how prevailing ENSO and IOD forcing or their preconditioning shape precipitation distribution in SA (Crétat et al., 2019; Gore et al., 2020; Howard et al., 2019; Ibebuchi, 2023b; Manatsa et al., 2012; Reason & Jagadheesha, 2005; Reason & Rouault, 2002); however, despite its proximity, IOPD's role is currently unknown. The three modes exhibit varying contemporaneous correlations throughout the year (Figure 2a). The strongest and most consistent is the relationship between ENSO and IOPD, which peaks in boreal winter. ENSO also correlates with IOD in the latter half of the year, but this correlation is mostly insignificant after accounting for the effect of IOPD on their relationship, indicating that IOPD acts as a mechanism for physically connecting SST variability in the Pacific and Indian oceans. The relationship between IOD and IOPD is strongest during the fall season.

The contemporaneous simple Pearson correlations of the three modes with monsoon precipitation over SA suggest a similar dipolar influence by ENSO and IOPD, transitioning between negative in the south and positive in the north around 15°S (Figure 2b). Most of the IOD's influence is positive but statistically significant only in areas north of Mozambique. The similarity between ENSO and IOPD is remarkable but not surprising. In a recent study, it was determined that ENSO's influence on boreal winter precipitation variability over some regions is primarily driven by atmospheric diabatic heating anomalies caused by ENSO-driven precipitation variability in the IO because of the strong coupling between IOPD and ENSO at a seasonal scale (Abid et al., 2023; Horan et al., 2023). This is also true in SA, where the direct influence of contemporaneous ENSO forcing on monsoon precipitation becomes insignificant after controlling for the effects of IOPD and IOD (Figure 2b). IOD, in contrast, becomes a significant positive forcing over SA after controlling for ENSO and IOPD, while IOPD's influence remains mostly unchanged over SA's eastern half, north of SICZ, after controlling for ENSO and IOD.

Our analysis shows that predicting monsoon precipitation in SA with significant skill is possible using ENSO, IOD, and IOPD precursors. We demonstrate this by examining the preconditioning of these natural modes in December, October, and July as predictors of the summer (DJF) monsoon in SA. First, we examine their lead simple Pearson and partial correlations with SA's monsoon precipitation to explain their predictive power (Figure 2c, S4). The strength of correlations among the three modes varies during these months (Figure 2a), resulting in different contributions to SA's precipitation predictability. In July, correlations between the three natural modes are weaker, which means each mode can have a more distinct and independent role in predicting monsoon precipitation. ENSO and IOPD lead correlations retain dipolar patterns like their contemporaneous correlations (Figure 2c, dotted red). However, unlike ENSO's limited contemporaneous role, controlling for IOD and IOPD retains most of its lead correlation, except for southeast SA, north of SICZ, where lead IOPD forcing has a more significant negative impact (Figure 2c, solid red). The July IOD shows precipitation controls like those in its contemporaneous relationship with the SA monsoon. In October, the strongest IOPD-IOD coupling is observed (Figure 2a). As a result, the October IOD exhibits a dipolar correlation with precipitation, like ENSO and IOPD (Figure 2c; dotted blue, Figure S4). After controlling for the other two factors, the IOPD correlation becomes mostly negative, while the IOD correlation becomes positive. ENSO retains a dipolar influence pattern. In December, dipolar patterns persist, although IOD's negative influence is relatively insignificant (Figure S4). ENSO (IOD) partial correlations with the precipitation are mostly negative (positive), while the IOPD relationship remains dipolar (Figure 2c; solid green). These analyses suggest that all three forcings play a role in monsoon variability in SA, and their interplay helps determine its predictability.

Next, we construct an MLR model using ENSO, IOD, and IOPD as independent variables or predictors and gridded precipitation over SA as the dependent variable to examine the extent to which precipitation variability can be explained through their contemporary forcings or preconditioning. Given the latitudinal contrast in their influences, the results are presented spatially (Figure S5) and in zonal averages (Figure 3). Several key points from this analysis can be summarized: 1) The strong coupling between ENSO and IOPD in DJF eliminates the independent role of contemporary ENSO forcing on monsoon precipitation beyond what is already propagated by IOPD (Figure 3b; black). As for the ENSO preconditioning, its predictive power is also the weakest, with statistically significant influence limited to SA's northernmost and southernmost parts (Figure 3c; black, Figure S5). 2) The IOD influence is predominantly positive and significant across all latitudes in DJF and with December preconditioning. However, its most robust influence is limited to the northernmost parts, with July and October preconditioning (Figure 3a; blue and red). The IOPD is the most prominent force, exerting strong dipolar influence in the north (positive; 5°S–12°S) and south (negative; 17°S–25°S), except in October when strong coupling with IOD limits its distinct role in predicting SA monsoon. Spatiotemporally varying roles of these natural forcings suggest that they can counteract or amplify one another's effect.

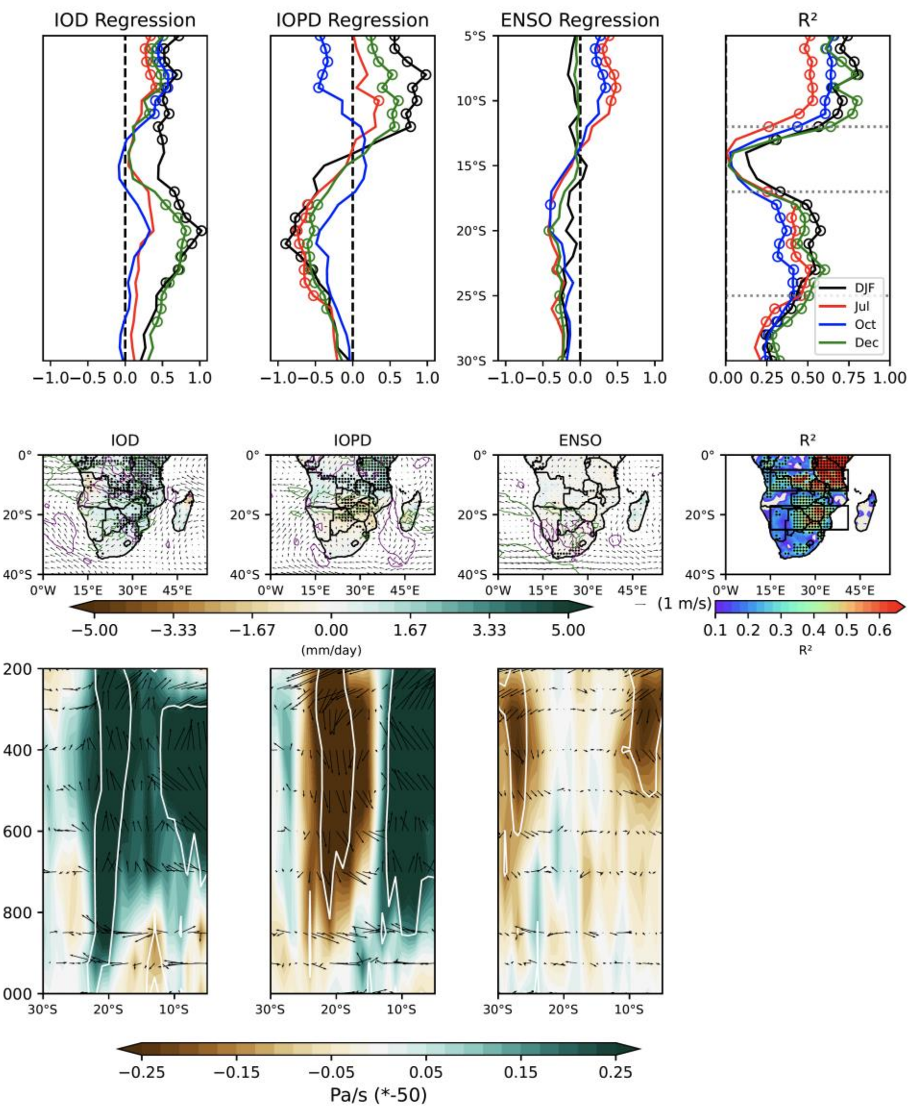

Figure 3. Zonally averaged partial regression coefficients of contemporaneous and lead (December, October, and July) IOD (a), IOPD (b), and ENSO (c) forcings in DJF precipitation multi-linear regression (MLR) models. Circles indicate statistical significance. d) The R^2 for MLR models in (a-c). (e-g) Same as in (a-c; black) but shown spatially for contemporaneous forcings-based MLR for DJF precipitation (colors) and 850 hPa winds (vectors). Green (purple) contours represent the statistical significance of the zonal (meridional) winds regression coefficient. h) The R^2 for the MLR model in (e-g). Black boxes indicated northern and southern regions. (i-k) Same as in (e-g) but for the zonally averaged vertical cross-section of DJF divergence (multiplied by 10E6) and vertical pressure velocity (multiplied by -50), shown as vectors. The regression coefficients related to vertical pressure velocity are also shown in color. White contours represent the statistical significance of colored contours. Statistical significance is at p<.05.

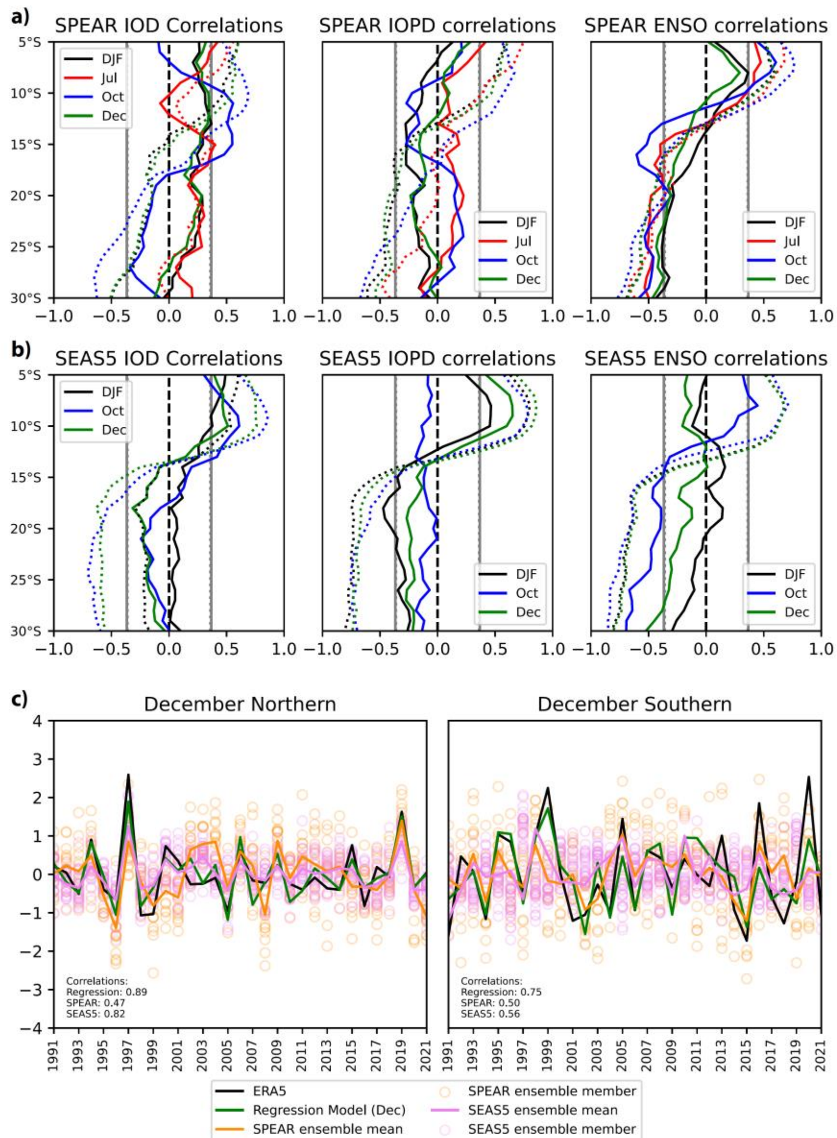

Figure 4. Zonally averaged partial (solid) and Pearson (dotted) correlation between DJF precipitation (5°E–52°E, land points) and contemporaneous and lead indexes of IOD (left), IOPD (center), and ENSO (right) in (a) SPEAR and (b) SEAS5. The vertical lines represent statistical significance (p<.05). c) The mean area-averaged precipitation over northern (left) and southern (right) parts of Southern Africa (rectangles in Figure 3h) in ERA5 (black), MLR model (green), SPEAR (orange) ensemble mean, and SEAS5 (violet) ensemble mean. The empirical (dynamical) models represent December forcings (initializations). Light circles indicate ensemble members in SPEAR and SEAS5.

Overall, the empirical model explains ~50% to >75% (~35% to >50%) zonally averaged precipitation variability in areas along the 5°S–12°S (17°S–25°S). Spatially, the skill is notably higher in southern Kenya and Tanzania, certain parts of Zambia, and within the region north of SICZ, encompassing parts of Mozambique, Zimbabwe, and Botswana (Figure S5). However, between 12°S and 17°S, predictability is limited due to the fluctuation between negative and positive influences and inherent low precipitation variability (Figures 1b, 3a). Regions with low predictability skills include northern Mozambique, central Zambia, southern Malawi, and southern Angola.

How do these natural modes of variability influence the monsoon circulation that eventually impacts precipitation? We explain it by regressing three-dimensional divergence, vertical pressure velocity, and 850 hPa winds onto ENSO, IOD, and IOPD indexes. In DJF, IOD enhances the moist flow in the lower atmosphere from continental Africa and the warm IO through the Mozambique Channel and strengthens the deep convective environment throughout the region except over Angola, where lower-level subsidence induced by the IOD suppresses convection (Figure 3b, 3c). Overall, these dynamic anomalies lead to widespread enhanced precipitation. IOPD, on the other hand, weakens MCT and SICZ, limiting moist flow over southeast Africa and reducing precipitation. In areas south (north) of 15°S, it suppresses (intensifies) the deep convective monsoon environment, weakening the southward seasonal march of moist continental air. ENSO's most significant influence is over South Africa, which enhances dry air entrainment from the southern Atlantic Ocean and reduces precipitation. It otherwise has limited influence on the background monsoonal environment. Accordingly, DJF atmospheric responses to ENSO, IOD, and IOPD July and October preconditioning provide a physical explanation of their leading relationships with precipitation over southern Africa, as shown in Figures 2, 3, S5, and S7.

We will now examine two seasonal forecasting systems, SPEAR and SEAS5, for their skillfullness in predicting monsoon precipitation over SA within the context of the three identified forcings. We begin by analyzing correlations between the modes and note that models' ensemble mean can represent their varying relationships. For instance, the IOD–IOPD correlation is strongest in October (SEAS5=0.89; SPEAR=0.89), as seen in reanalyses (ERA5 = 0.86). Similarly, the ENSO–IOPD coupling increases in December (SEAS5=0.81; SPEAR=0.74), consistent with reanalyses (ERA5 = 0.75). July's initialized SPEAR ensemble mean also shows a relatively weak correspondence between the three modes. Note that SEAS5 does not provide forecast data for DJF with the July initialization. However, models exhibit biases in representing the influence of these modes on SA monsoon variability. The biases are particularly severe in SPEAR. Compared to SEAS5, it lacks skill in representing the dipolar pattern of lead Pearson correlations of three indexes with DJF precipitation (Figures 4, S8, S9). Additionally, SPEAR and SEAS5 exhibit an overly strong influence of ENSO on precipitation variability across SA. They show no significant influence of IOPD over SA's southeast in partial correlations after accounting for the effects of IOD and ENSO (Figures 4, S8, S9), which contrasts with reanalyses (Figures 2, S4). Similarly, IOD's positive association over latitudes south of 17°S is also missing in its partial correlations (Figures 2, 4). Both models show a negative IOD relationship instead. On the other hand, ENSO's partial correlations are overly strong in both cases. SPEAR also fails to accurately represent the IOD and IOPD lead influences in July initialized simulations.

Given the modeling errors in representing IOD, IOPD, and ENSO teleconnection across SA during monsoon, its predictability is lower in dynamical models than in the empirical model. Because of the contrasting influences of the three modes along the latitude, we assess the predictability of two seasonal forecasting systems by analyzing time series of area average precipitation over two regions, one between 5°S and 12°S where influence is predominantly positive and one between 17°S and 25°S where influence is predominantly negative (Figures 4c, S10). The empirical model using ENSO, IOD, and IOPD as predictors separately for July, October, and December can account for 52%, 64%, and 79% of precipitation variance in the northern part. It can also explain 46%, 44%, and 58% of precipitation variance in the southern part. Please note that the empirical model does not suffer from overfitting, as the predicted R^2 closely follows the actual R^2 in all instances (Figure S11). While, by definition, the predicted R^2 is always lower than the actual R2, a significant difference between the two could indicate an overfitting issue in the MLR model.

Due to strong coupling with IOD, IOPD loses most of its independent influence over the southern part with October preconditioning. This results in a lower predictability with the October lead. SPEAR-explained precipitation variance is 26%, 38%, and 25% in the northern part and 0%, 25%, and 23% in the southern part with July, October, and December initializations. Similarly, SEAS5-explained precipitation variance is 56% and 69% in the northern part and 46% and 34% in the southern part with October and December initializations. The substantially lower skill in SPEAR compared to SEAS5 is due to its much lower skill in representing the influences of IOD and IOPD over both areas and ENSO influence over the southern parts (Figure 4).

4 Summary

We have constructed an empirical model using three natural climate variability modes related to SST and precipitation variability in the Pacific and Indian oceans (ENSO, IOD, IOPD). This model effectively explains precipitation variance across SA during the core monsoon season. Furthermore, these natural modes can also be utilized to predict monsoon precipitation in SA with a five-month lead time. The three modes exhibit varying coupling strengths throughout the year. For instance, IOPD is strongly coupled with IOD in the fall and ENSO in the winter. These interdependencies between the three modes influence their distinct roles in shaping precipitation variability over SA. A major component of ENSO's contemporaneous teleconnection with SA is indirectly through its coupling with IOPD in the IO. Direct ENSO forcing does not contribute anything substantial beyond IOPD's teleconnection pattern. IOPD's forcing is a major contributor to precipitation predictability with different lead times. Its weakest predictive power is in October because of the strong coupling between IOD and IOPD, which limits IOPD's distinct role.

The SEAS5 and SPEAR models provide accurate information on varying monthly correlations between ENSO, IOD, and IOPD. They also capture ENSO and IOPD interannual variability precisely. However, their ability to describe IOD's interannual variability is less effective. Moreover, SPEAR shows a poor simulation of their teleconnections in SA, particularly below 17°S. As a result, both models underperform compared to the empirical model, with SPEAR being the least effective in SA’s southeast. These findings highlight the importance of accurately representing ENSO, IOD, and IOPD teleconnections to enhance predictability in seasonal forecasting systems during the summer monsoon in SA.

Acknowledgments

This research used the OLCF resources, a DOE Office of Science User Facility supported under Contract DE-AC05-00OR22725. This work is supported by the U.S. Air Force Numerical Weather Modeling Program and NCCR Center, located within the NNCCS at the ORNL and supported under a Strategic Partnership Project 2316T849-08 between DOE and NOAA.

Author contributions:

M.F.H. and M.A. designed the study. M.F.H. performed the analyses. All authors were involved in the discussion of results. M.A. and M.F.H. wrote the manuscript draft and finalized it with feedback from all authors.

Competing interests:

The authors declare that they have no competing interests.

Data and materials availability:

All datasets used in this analysis are publicly available. The ERA5 reanalysis and SEAS5 model data are available from the Copernicus Climate Change Service (C3S) Climate Date Store (https://cds.climate.copernicus.eu/). SPEAR data is available from the North American Multi-model Ensemble archive (http://iridl.ldeo.columbia.edu/SOURCES/.Models/.NMME/.GFDL-SPEAR/). CPC Data is available from NOAA's Physical Sciences Laboratory

(https://psl.noaa.gov/data/gridded/data.cpc.globalprecip.html). CRU Data is available from the climactic research unit (https://crudata.uea.ac.uk/cru/data/hrg/). The analysis codes will be provided upon acceptance of the manuscript.

References

Abid, M. A., Ashfaq, M., Kucharski, F., Evans, K. J., & Almazroui, M. (2020). Tropical Indian Ocean Mediates ENSO Influence Over Central Southwest Asia During the Wet Season. *Geophysical Research Letters*, *47*(18), e2020GL089308. https://doi.org/10.1029/2020GL089308

Abid, M. A., Kucharski, F., Molteni, F., & Almazroui, M. (2023). Predictability of Indian Ocean precipitation and its North Atlantic teleconnections during early winter. *Npj Climate and Atmospheric Science*, *6*(1), 17. https://doi.org/10.1038/s41612-023-00328-z

De Andrade, F. M., Young, M. P., Macleod, D., Hirons, L. C., Woolnough, S. J., & Black, E. (2021). Subseasonal Precipitation Prediction for Africa: Forecast Evaluation and Sources of Predictability. *Weather and Forecasting*, *36*(1), 265–284. https://doi.org/10.1175/WAF-D-20-0054.1

Ashfaq, M., Cavazos, T., Reboita, M. S., Torres-Alavez, J. A., Im, E. S., Olusegun, C. F., et al. (2020). Robust late twenty-first century shift in the regional monsoons in RegCM-CORDEX simulations. *Climate Dynamics 2020 57:5*, *57*(5), 1463–1488. https://doi.org/10.1007/S00382-020-05306-2

Barimalala, R., Blamey, R. C., Desbiolles, F., & Reason, C. J. C. (2020). Variability in the Mozambique Channel Trough and Impacts on Southeast African Rainfall. *Journal of Climate*, *33*(2), 749–765. https://doi.org/10.1175/JCLI-D-19-0267.1

Behera, S. K., & Yamagata, T. (2001). Subtropical SST dipole events in the southern Indian Ocean. *Geophysical Research Letters*, *28*(2), 327–330. https://doi.org/10.1029/2000GL011451

Cook, K. H. (2000). The South Indian Convergence Zone and Interannual Rainfall Variability over Southern Africa. *Journal of Climate*, *13*(21), 3789–3804. https://doi.org/10.1175/1520-0442(2000)013

Crétat, J., Pohl, B., Dieppois, B., Berthou, S., & Pergaud, J. (2019). The Angola Low: relationship with southern African rainfall and ENSO. *Climate Dynamics*, *52*(3–4), 1783–1803. https://doi.org/10.1007/s00382-018-4222-3

Delworth, T. L., Cooke, W. F., Adcroft, A., Bushuk, M., Chen, J. H., Dunne, K. A., et al. (2020). SPEAR: The Next Generation GFDL Modeling System for Seasonal to Multidecadal Prediction and Projection. *Journal of Advances in Modeling Earth Systems*, *12*(3), e2019MS001895. https://doi.org/10.1029/2019MS001895

Driver, P., & Reason, C. J. C. (2017). Variability in the Botswana High and its relationships with rainfall and temperature characteristics over southern Africa. *International Journal of Climatology*, *37*, 570–581. https://doi.org/10.1002/JOC.5022

Eade, R., Smith, D., Scaife, A., Wallace, E., Dunstone, N., Hermanson, L., & Robinson, N. (2014). Do seasonal-to-decadal climate predictions underestimate the predictability of the real world? *Geophysical Research Letters*, *41*(15), 5620–5628. https://doi.org/10.1002/2014GL061146

Geppert, M., Hartmann, K., Kirchner, I., Pfahl, S., Struck, U., & Riedel, F. (2022). Precipitation Over Southern Africa: Moisture Sources and Isotopic Composition. *Journal of Geophysical Research: Atmospheres*, *127*(21), e2022JD037005. https://doi.org/10.1029/2022JD037005

Gore, M., Abiodun, B. J., & Kucharski, F. (2020). Understanding the influence of ENSO patterns on drought over southern Africa using SPEEDY. *Climate Dynamics*, *54*(1–2), 307–327. https://doi.org/10.1007/S00382-019-05002-W/FIGURES/15

Harris, I., Osborn, T. J., Jones, P., & Lister, D. (2020). Version 4 of the CRU TS monthly high-resolution gridded multivariate climate dataset. *Scientific Data 2020 7:1*, *7*(1), 1–18. https://doi.org/10.1038/s41597-020-0453-3

Hersbach, H., Bell, B., Berrisford, P., Hirahara, S., Horányi, A., Muñoz-Sabater, J., et al. (2020). The ERA5 global reanalysis. *Quarterly Journal of the Royal Meteorological Society*, *146*(730), 1999–2049. https://doi.org/10.1002/qj.3803

Hoell, A., Funk, C., Zinke, J., & Harrison, L. (2017). Modulation of the Southern Africa precipitation response to the El Niño Southern Oscillation by the subtropical Indian Ocean Dipole. *Climate Dynamics*, *48*(7–8), 2529–2540. https://doi.org/10.1007/s00382-016-3220-6

Horan, M., Kucharski, F., Johnson, N., & Ashfaq, M. (2023). Winter precipitation predictability in Central Southwest Asia and its representation in seasonal forecast systems. https://doi.org/10.21203/RS.3.RS-3079978/V1

Howard, E., & Washington, R. (2019). Drylines in Southern Africa: Rediscovering the Congo Air Boundary. *Journal of Climate*, *32*(23), 8223–8242. https://doi.org/10.1175/JCLI-D-19-0437.1

Howard, E., Washington, R., & Hodges, K. I. (2019). Tropical Lows in Southern Africa: Tracks, Rainfall Contributions, and the Role of ENSO. *Journal of Geophysical Research: Atmospheres*, *124*(21), 11009–11032. https://doi.org/10.1029/2019JD030803

Ibebuchi, C. C. (2023a). Circulation Patterns Linked to the Positive Sub-Tropical Indian Ocean Dipole. *Advances in Atmospheric Sciences*, *40*(1), 110–128. https://doi.org/10.1007/s00376-022-2017-2

Ibebuchi, C. C. (2023b). Patterns of atmospheric circulation linking the positive tropical Indian Ocean dipole and southern African rainfall during summer. *Journal of Earth System Science*, *132*(1), 13. https://doi.org/10.1007/s12040-022-02025-6

Johnson, S. J., Stockdale, T. N., Ferranti, L., Balmaseda, M. A., Molteni, F., Magnusson, L., et al. (2019). SEAS5: The new ECMWF seasonal forecast system. *Geoscientific Model Development*, *12*(3), 1087–1117. https://doi.org/10.5194/GMD-12-1087-2019

Landman, W. A., & Beraki, A. (2012). Multi-model forecast skill for mid-summer rainfall over southern Africa. *International Journal of Climatology*, *32*(2), 303–314. https://doi.org/10.1002/JOC.2273

Landman, W. A., Dewitt, D., Lee, D. E., Beraki, A., & Lötter, D. (2012). Seasonal Rainfall Prediction Skill over South Africa: One- versus Two-Tiered Forecasting Systems. *Weather and Forecasting*, *27*(2), 489–501. https://doi.org/10.1175/WAF-D-11-00078.1

Manatsa, D., Reason, C. J. C., & Mukwada, G. (2012). On the decoupling of the IODZM from southern Africa Summer rainfall variability. *International Journal of Climatology*, *32*(5), 727–746. https://doi.org/10.1002/joc.2306

Mehmood, S., Ashfaq, M., Kapnick, S., Gosh, S., Abid, M. A., Kucharski, F., et al. (2022). Dominant controls of cold-season precipitation variability over the high mountains of Asia. *Npj Climate and Atmospheric Science 2022 5:1*, *5*(1), 1–13. https://doi.org/10.1038/s41612-022-00282-2

Monerie, P. A., Robson, J., Dong, B., Dieppois, B., Pohl, B., & Dunstone, N. (2019). Predicting the seasonal evolution of southern African summer precipitation in the DePreSys3 prediction system. *Climate Dynamics*, *52*(11), 6491–6510. https://doi.org/10.1007/S00382-018-4526-3/FIGURES/3

Mpungose, N., Thoithi, W., Blamey, R. C., & Reason, C. J. C. (2022). Extreme rainfall events in southeastern Africa during the summer. *Theoretical and Applied Climatology*, *150*(1–2), 185–201. https://doi.org/10.1007/s00704-022-04162-w

Mukherjee, S., Ashfaq, M., & Mishra, A. K. (2020). Compound Drought and Heatwaves at a Global Scale: The Role of Natural Climate Variability-Associated Synoptic Patterns and Land-Surface Energy Budget Anomalies. *Journal of Geophysical Research: Atmospheres*, *125*(11), e2019JD031943. https://doi.org/10.1029/2019JD031943

Munday, C., & Washington, R. (2017). Circulation controls on southern African precipitation in coupled models: The role of the Angola Low. *Journal of Geophysical Research: Atmospheres*, *122*(2), 861–877. https://doi.org/10.1002/2016JD025736

Osman, M., & Vera, C. S. (2017). Climate predictability and prediction skill on seasonal time scales over South America from CHFP models. *Climate Dynamics*, *49*(7–8), 2365–2383. https://doi.org/10.1007/S00382-016-3444-5/FIGURES/14

Reason, C. J. C. (2001). Subtropical Indian Ocean SST dipole events and southern African rainfall. *Geophysical Research Letters*, *28*(11), 2225–2227. https://doi.org/10.1029/2000GL012735

Reason, C. J. C., & Jagadheesha, D. (2005). A model investigation of recent ENSO impacts over southern Africa. *Meteorology and Atmospheric Physics*, *89*(1–4), 181–205. https://doi.org/10.1007/S00703-005-0128-9/METRICS

Reason, C. J. C., & Rouault, M. (2002). ENSO-like decadal variability and South African rainfall. *Geophysical Research Letters*, *29*(13), 16–1. https://doi.org/10.1029/2002GL014663

Reason, C. J. C., Landman, W., & Tennant, W. (2006). Seasonal to Decadal Prediction of Southern African Climate and Its Links with Variability of the Atlantic Ocean. *Bulletin of the American Meteorological Society*, *87*(7), 941–956. https://doi.org/10.1175/BAMS-87-7-941

Saji, N. H., Goswami, B. N., Vinayachandran, P. N., & Yamagata, T. (1999). A dipole mode in the tropical Indian ocean. *Nature*, *401*(6751), 360–363. https://doi.org/10.1038/43854

Scaife, A. A., Arribas, A., Blockley, E., Brookshaw, A., Clark, R. T., Dunstone, N., et al. (2014). Skillful long-range prediction of European and North American winters. *Geophysical Research Letters*, *41*(7), 2514–2519. https://doi.org/10.1002/2014GL059637

Silvério, K. C., & Grimm, A. M. (2022). Southern African monsoon: intraseasonal variability and monsoon indices. *Climate Dynamics*, *58*(3–4), 1193–1220. https://doi.org/10.1007/s00382-021-05954-y

Wetterhall, F., Winsemius, H. C., Dutra, E., Werner, M., & Pappenberger, F. (2014). Seasonal predictions of agro-meteorological drought indicators Seasonal predictions of agro-meteorological drought indicators for the Limpopo basin Seasonal predictions of agro-meteorological drought indicators. *Hydrol. Earth Syst. Sci. Discuss*, *11*, 861–888. https://doi.org/10.5194/hessd-11-861-2014

Winsemius, H. C., Dutra, E., Engelbrecht, F. A., Archer Van Garderen, E., Wetterhall, F., Pappenberger, F., & Werner, M. G. F. (2014). The potential value of seasonal forecasts in a changing climate in southern Africa. *Hydrology and Earth System Sciences*, *18*(4), 1525–1538. https://doi.org/10.5194/HESS-18-1525-2014

Xie, P., Yatagai, A., Chen, M., Hayasaka, T., Fukushima, Y., Liu, C., & Yang, S. (2007). A Gauge-Based Analysis of Daily Precipitation over East Asia. *Journal of Hydrometeorology*, *8*(3), 607–626. https://doi.org/10.1175/JHM583.1